In Situ Observation of Nonpolar to Strongly Polar Atom-Ion Collision Dynamics

M. Berngruber,[1,*] D. J. Bosworth[2,3,*,†] O. A. Herrera-Sancho[1,4,5,6] V. S. V. Anasuri,[1] N. Zuber,[1]
F. Hummel[7,‖] J. Krauter,[1] F. Meinert[1] R. Löw,[1] P. Schmelcher[2,3,‡] and T. Pfau[1,§]

[1]*5. Physikalisches Institut, Universität Stuttgart, Pfaffenwaldring 57, 70569 Stuttgart, Germany*
[2]*Zentrum für Optische Quantentechnologien, Universität Hamburg, Luruper Chaussee 149, 22761 Hamburg, Germany*
[3]*Hamburg Centre for Ultrafast Imaging, Universität Hamburg, Luruper Chaussee 149, 22761 Hamburg, Germany*
[4]*Escuela de Física, Universidad de Costa Rica, 2060 San Pedro, San José, Costa Rica*
[5]*Instituto de Investigaciones en Arte, Universidad de Costa Rica, 2060 San Pedro, San José, Costa Rica*
[6]*Centro de Investigación en Ciencias Atómicas, Nucleares y Moleculares,*
Universidad de Costa Rica, 2060 San Pedro, San José, Costa Rica
[7]*Max-Planck-Institute for the Physics of Complex Systems, Nöthnitzer Straße 38, 01187 Dresden, Germany*

The onset of collision dynamics between an ion and a Rydberg atom is studied in a regime characterized by a multitude of collision channels. These channels arise from coupling between a nonpolar Rydberg state and numerous highly polar Stark states. The interaction potentials formed by the polar Stark states show a substantial difference in spatial gradient compared to the nonpolar state leading to a separation of collisional timescales, which is observed *in situ*. For collision energies in the range of $k_B\mu$K to k_BK, the dynamics exhibit a counterintuitive dependence on temperature, resulting in faster collision dynamics for cold—initially "slow"—systems. Dipole selection rules enable us to prepare the collision pair on the nonpolar potential in a highly controlled manner, which determines occupation of the collision channels. The experimental observations are supported by semiclassical simulations, which model the pair state evolution and provide evidence for tunable nonadiabatic dynamics.

DOI: 10.1103/PhysRevLett.133.083001

Introduction—Observing, understanding, and controlling individual collisions are prerequisites for many-body physics based on atoms or molecules. Especially in the ultracold regime, where collisions between neutral atoms can be engineered by Feshbach resonances, a high level of control is reached [1]. This makes it possible to study, for example, the study of degenerate molecular gases [2,3], Feshbach molecules [4,5], and Efimov physics [6]. However, when it comes to collisions between charged and neutral particles, reaching the same level of quantum control becomes harder since the range of interactions increases, thus requiring even lower temperatures to reach the quantum regime of scattering [7,8]. More exotic collisions can be studied in systems of laser-cooled Rydberg atoms, which have the advantage of showing long-range interactions, allowing collisions to occur on larger length, slower time, and lower energy scales, making them easier to observe with spatial and temporal resolution. Even exotic bound states between a Rydberg atom and neutral ground state atoms forming ultralong-range molecules have been observed [9–12]. Moreover, the complex Rydberg level structure can give rise to intriguingly rich potential energy surfaces with avoided crossings and conical intersections providing means to study effects beyond the Born-Oppenheimer approximation [13,14].

More recently, also systems combining Rydberg atoms and ions have become an active field of research [15–21]. Here, we pursue this direction and explore the dynamical processes that lead to a multichannel collision between an ion and a Rydberg atom. Instead of an ion trap we rely on compensating electric fields to work with free-floating ions in an almost net-zero electric field environment. Our high-resolution ion microscope allows us to study collisional dynamics with both spatial and temporal resolution. We are therefore not restricted to only analyzing the initial and final collision partners, but may instead directly observe the dynamics as the collision unfolds.

Theory—The polarizability of highly excited Rydberg atoms gives rise to a long-range charge-induced dipole interaction potential which is shown as a function of the internuclear distance R for the specific case of the $|129S\rangle$ state in Fig. 1. These potential energy curves (PECs) are calculated by exact diagonalization of the electronic Hamiltonian $H_e = H_0 + V_I(R)$, where H_0 describes the unperturbed Rydberg atom and V_I the ion-Rydberg interaction. This interaction term can be written in a multipole
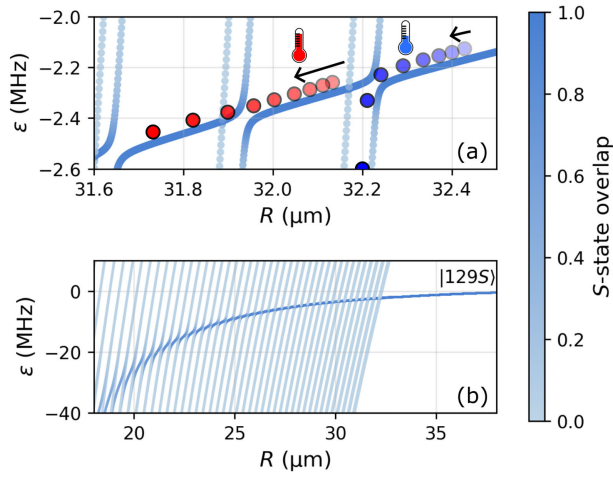

FIG. 1. Ion-Rydberg collision channels. Adiabatic potential energy curves obtained via exact diagonalization of the electronic Hamiltonian (see Ref. [22]). (a) Close-up around the avoided crossings near the nonpolar $|129S\rangle$ atomic Rydberg state, illustrating the presence of initially slow (red) and fast (blue) collision channels. Counterintuitively, occupation of the fast channels is more probable for initially slower particles. (b) Larger-scale plot of the avoided crossings between the nonpolar S-state and multiple strongly polar Stark states from the neighboring asymptotically degenerate hydrogenic manifold. The overlap of the electronic states with the unperturbed $|129S\rangle$ atomic Rydberg state is denoted by the colorbar. Energies are given relative to the $|129S\rangle$ atomic Rydberg state.

expansion, where we consider terms up to the sixth order (see Ref. [22]). One can distinguish between two regions: the first region is defined in the asymptotic limit for large R, where the potential of the nonpolar S-state falls off with $1/R^4$ due to the charge-induced dipole interaction between the ion and the atomic Rydberg S-state; the second region is found at $R \lesssim 33$ μm for the case of $|129S\rangle$, which is nevertheless approximately 26 times larger than the size of the Rydberg orbit. Here, the ion-induced Stark shift becomes large enough that strongly polar, large angular momentum states from the neighboring $n = 126$ hydrogenic manifold start to cross into the polarization potential and form a series of avoided crossings. For Rydberg S-states in ^{87}Rb, the polarization potential strictly decreases in energy while approaching the ion such that the two collision partners will always be accelerated toward each other. In the direct vicinity of these avoided crossings, the Born-Oppenheimer (BO) approximation is no longer suitable to describe the dynamics properly. Instead, a nonadiabatic, semiclassical model using the Landau-Zener (LZ) formula is employed [28]. This allows us to estimate the probability for an adiabatic transition to a strongly polar state at each crossing and thus can be used to predict the occupation of the different collision channels. The probability P_{ij} to transition nonadiabatically from PEC i to an adjacent curve j is given by $P_{ij} = \exp(-2\pi a_{ij}^2/(\dot{R}\alpha_{ij}))$ [29], where a_{ij} is half the energy gap between the adiabatic PECs at the avoided

crossing and α_{ij} is the differential gradient between the diabatic PECs.

From this formula, it is clear that the probability of undergoing adiabatic dynamics at a given crossing can be experimentally tuned through the relative velocity $\dot{R}$, which is determined in an experimental setting by the atom temperature and the additional kinetic energy acquired upon falling inward on the polarization potential of the nonpolar S-state. Therefore, systems with small relative velocities have an increased probability to follow the PEC adiabatically. In contrast, systems with high relative velocities have a larger probability to traverse the crossing nonadiabatically and thereby remain on the comparatively flat polarization potential. Hence, each avoided crossing provides two collisional channels: one that is mostly populated by systems with low kinetic energy (cold channel) and one that is mostly occupied by high kinetic energy systems (hot channel), see Fig. 1. Interestingly, this leads to a counterintuitive behavior for the overall dynamics: if a cold, low kinetic energy system follows the PEC adiabatically, it will ultimately reach the steep strongly polar potential and thus rapidly accelerate. This results in a faster collision compared to a system with high kinetic energy, which travels along the flat S-state potential and experiences weaker acceleration.

Overview of experimental sequence—The charged ion-Rydberg atom system is realized in a laser-cooled rubidium cloud held in an optical dipole trap of a temperature of about 20 μK. In order to minimize stray electric fields in the system, six electrodes are used to compensate fields well below 100 μV/cm [30]. In that way, the ions can be kept in position for the time of the experiment and no ion trap is needed. An experimental block starts with a 1 μs long ionization pulse, which incorporates a two-photon ionization process, providing just enough energy to overcome the ionization threshold [see Fig. 2(a)]. Next, a Rydberg atom is excited in the electric field of the ion by using a 1 μs long Rydberg excitation pulse, again involving two laser beams [see Fig. 2(b)]. The detuning Δ of the upper 480 nm excitation laser from the bare atomic state in zero field determines the initial radius R_0 at which the Rydberg atom is facilitated around the ion. The radial distribution has a width that is given by the effective linewidth of the two-photon excitation. The verlocity $\dot{R}_0$ is mostly determined by the temperature of the rubidium cloud. This blue laser illuminates the atomic cloud as a thin light sheet in the horizontal direction, thus confining the system for highly excited Rydberg states to a quasi-2D plane, leading to the facilitation of Rydberg atoms located on a ring around the ion (for further details, see Ref. [22]). Afterwards a variable time t_{dyn} can be applied allowing the system to evolve freely. In order to detect the two particles in a distinguishable way, we drag the ion along the optical axis of the ion microscope without displacing it in the imaging plane. To do so, two field electrodes are used to apply a weak electric field of about 1.1 V/cm, which is
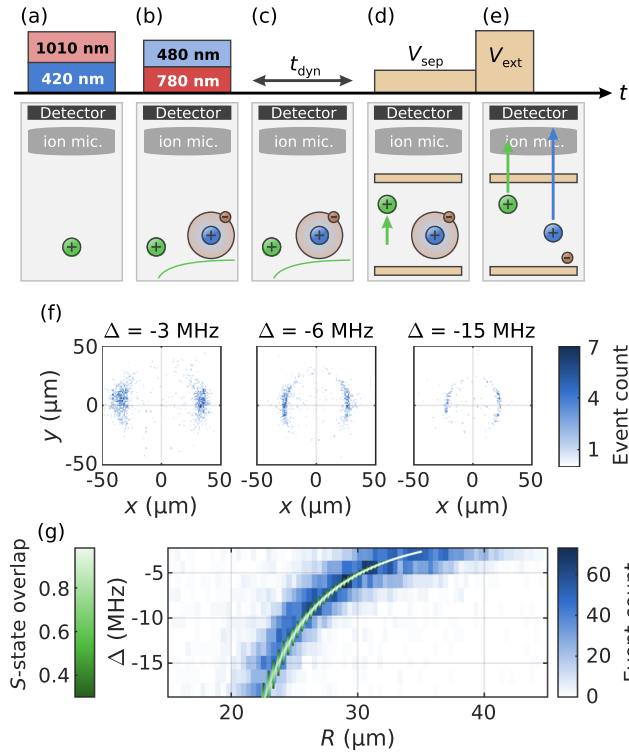
FIG. 2. Experimental sequence and initial state preparation. (a)–(e) Schematics of the experimental sequence, which consists of the following steps: (a) two-photon ionization to create an ion, (b) two-photon Rydberg excitation in the electric field of the ion, (c) variable interaction time, (d) applying a small separation field which drags the ion along the optical axis of the ion microscope, (e) ionization of the Rydberg atom and imaging of both particles by using a large electric field. Panel (f) shows the Rydberg atom position relative to the ion (located at the origin) for different Rydberg laser detunings Δ from the bare $|129S\rangle$ state in absence of an ion. (g) Histograms of the azimuthally averaged ion-Rydberg atom distance R for various detunings Δ (blue). The theoretically calculated polarization potential is shown in the white to green color code, which indicates the overlap with the bare $|129S\rangle$ state (only overlaps ≥ 0.3 are shown).

small enough to not ionize the Rydberg atom [see Fig. 2(d)]. In the final detection step [Fig. 2(e)], a large electric field of 340 V/cm is applied to field-ionize the Rydberg atom and to accelerate both particles into the ion microscope. Because of the previous separation between the ion and the Rydberg atom, they will arrive at different times at the detector and are therefore easily distinguishable [21,31].

Results and discussion—If the interaction time t_{dyn} in Fig. 2(c) is set to zero, Rydberg atoms initially excited on the flat polarization potential can be directly detected at their original positions. Excitation to the high angular momentum curves is ruled out due to negligible D-state overlap. By scanning the detuning Δ of the Rydberg excitation we can spectroscopically map out the resonance condition for facilitated excitation on the interaction

potential. Figure 2(f) shows examples of averaged *in situ* images of the Rydberg atom position relative to the ion, meaning that the ion is always located at the origin. Owing to the excitation in a quasi-2D plane, a symmetric ring can be observed with the ion microscope. The upper and lower part are not populated due to the finite, elongated shape of the atomic cloud. As it can be clearly seen, the distance between the ion and the Rydberg atom decreases for larger detunings as expected from the facilitation process. Figure 2(g) summarizes the result of such *in situ* images by integrating over the azimuthal angle and showing the data as a function of the internuclear distance R, which represents a direct measurement of the $|129S\rangle$ ion-Rydberg pair state potential. The blue histogram shows the experimentally obtained data, which is in good agreement with the calculated PEC displayed in green.

In the next step, we introduce a variable interaction time $t_{\mathrm{dyn}} > 0$ between the Rydberg excitation and the detection, during which the dynamics take place. This allows the ion-Rydberg pair to move on the interaction potential, such that the system encounters the series of avoided crossings shown in Fig. 1(b). The top row of Fig. 3 shows results for the observed dynamics of the $|129S\rangle$ state at three different detunings. Δ' is the detuning relative to the outermost avoided crossing, such that for $\Delta' > 0$ the system is initialized outside the fan of the hydrogenic manifold. Each panel represents an average over at least 6500 ion-Rydberg events on the detector. Solid and dashed lines indicate the results of semiclassical simulations that account for effects due to finite temperature, effective laser linewidth, experimental timings, as well as the geometry of the setup. We model the observed ion-Rydberg pair dynamics by solving the pair's classical equation of motion along all possible collision channels. Each resulting trajectory is assigned a weight corresponding to the probability of following that particular channel, provided by the LZ formula (for further details, see Ref. [22]). We observe good agreement between the experimental results and the simulations. For negative Δ', one clearly observes faster dynamics overall due to the transition to steep, strongly polar states. At longer times, however, deviations appear which are due to short-range interaction processes. Notably, for $R \lesssim 5$ μm charge transfer of the Rydberg electron can occur. Such processes are beyond the scope of our model and their products cannot be filtered in the experiment.

Our semiclassical model can shed light on the significance of nonadiabatic transitions in the dynamics by studying the change in population of the slow and fast collision channels over time. The bottom row of Fig. 3 shows the population of the strongly polar states over time for LZ simulations (red) and fully adiabatic simulation based on individual, noncoupled PECs (blue). For all Δ', the population growth is slower for LZ simulations due to nonadiabatic transitions. A more quantitative comparison can be made by comparing the times t_e (dashed vertical
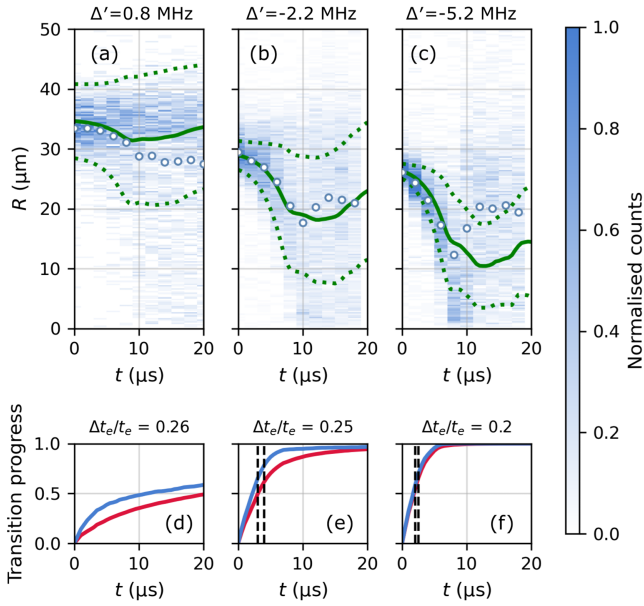
FIG. 3. Ion-Rydberg pair dynamics. (a)–(c) Observed relative atomic dynamics with results of LZ simulations overlaid for different detunings of the Rydberg laser Δ' relative to the outermost avoided crossing at $R \approx 32.2$ μm. The colorbar gives the number of measured counts as a fraction of counts at $t = 0$. Circular data points indicate the mean of the measured distribution for each time step. Solid (dotted) lines indicate the mean (standard deviation) of the theoretical distribution. (d)–(f) Population of the fast collision channels (strongly polar states) over time for both LZ (red) and adiabatic (blue) simulations. Dashed vertical lines (not visible for $\Delta' = 0.8$ MHz in this interval) indicate the time t_e at which the population reaches $1 - 1/e$ (approx. 63%). $\Delta t_e/t_e$ is the relative difference in this time between the LZ and adiabatic simulations. For details of the simulations, see Ref. [22].

lines) at which the population of the nonpolar S-state curve has decayed to $1/e$. The relative difference Δt_e in t_e decreases as the Rydberg atoms are excited further inside the fan, indicating that the motion becomes increasingly adiabatic. This is due to the growing gap size a_{ij} at the avoided crossings at smaller R (see Ref. [22]). In this way the timescale of the dynamics can also be controlled via the laser detuning.

Nonadiabatic transitions are further influenced by the gas temperature T. For high T, ion-Rydberg pairs have a larger probability to follow the slow collision channel due to their initially greater relative velocity. We illustrate this point theoretically in Fig. 4, which shows the transition to fast collision channels over time at different temperatures and two different laser detunings relative to the outermost avoided crossing. The relative difference in t_e increases with T for both detunings [see Fig. 4(d)], indicating that the pairs created in hotter gases spend more time on the slow collision channel created by the nonpolar S-state. Pairs gain kinetic energy as they fall inward along the polarization potential. For $\Delta'_1 = 0.06$ MHz, this gain in kinetic
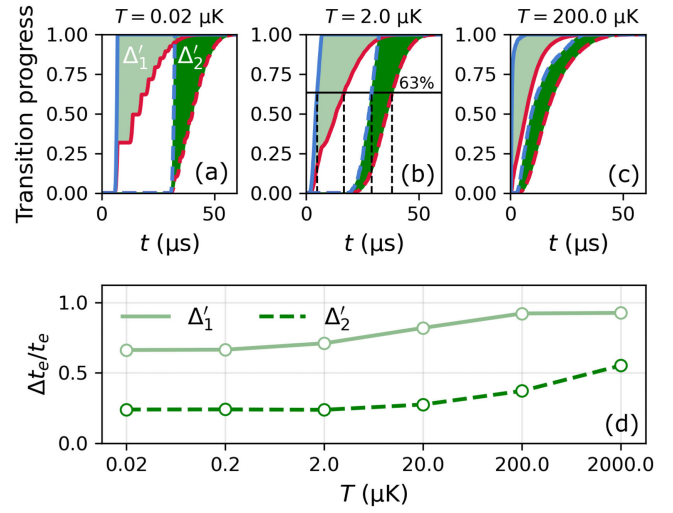

FIG. 4. Predicted impact of temperature on dynamics. Panels (a)–(c) show theoretical results which compare the population of fast collision channels (strongly polar states) over time for both LZ (red) and adiabatic (blue) simulations at different gas temperatures T. Solid (dashed) lines denote an initial laser detuning of $\Delta'_1 = 0.06$ MHz ($\Delta'_2 = 0.31$ MHz) relative to the outermost avoided crossing at $R \approx 32.2$ μm [see Fig. 1(b)]. Panel (d) shows the relative difference in t_e between LZ and adiabatic simulations over a range of gas temperatures. t_e is the time at which the polar state population reaches $1 - 1/e$ (approx. 63%), indicated for the case of $T = 2.0$ μK by the dashed vertical lines in (b).

energy corresponds to approximately 0.4 μKk_B of thermal energy, whilst $\Delta'_2 = 0.31$ MHz is equivalent to 2.0 μKk_B. This additional heating accounts for the negligible change in $\Delta t_e/t_e$ for temperatures below 2 μK [Fig. 4(d)].

Nonadiabatic transitions will also play a more significant role in the dynamics at higher n as a result of the narrowing avoided crossings, whose gap sizes a_{ij} follow a power-law decay with n (see Ref. [22]). The signal of nonadiabatic transitions can thus be enhanced by probing dynamics at larger n.

Summary and outlook—We studied the onset of collisional dynamics between an ion-Rydberg pair in a regime of multiple coupled channels with varying collision timescales. We were able to describe the experimentally observed dynamics with the help of a LZ model. Further, the simulations show that the collisional dynamics can not only be tuned by the initial distance but should also be tunable by other parameters like the principal quantum number. Our work has explored the role of nonadiabatic effects in ion-Rydberg collisions and lays the foundation for future explorations of beyond Born-Oppenheimer physics with Rydberg atoms, such as molecular dynamics in the presence of conical intersections. Precisely understanding nonadiabatic couplings in complicated potential energy landscapes is also a key ingredient to better predict the lifetime of Rydberg molecules such as macrodimers or ion-Rydberg molecules [14]. In this current experimental

realization, the ion-Rydberg complex was photoassociated directly out of a trapped gas of ^{87}Rb. Future experiments might consider using individually trapped atoms in a tweezer setup, which would offer more precise control over the initial separation of the ion-Rydberg pair, thereby further improving the starting conditions of the collision.

---

[1] C. Chin, R. Grimm, P. Julienne, and E. Tiesinga, Feshbach resonances in ultracold gases, Rev. Mod. Phys. **82**, 1225 (2010).

[2] L. De Marco, G. Valtolina, K. Matsuda, W. G. Tobias, J. P. Covey, and J. Ye, A degenerate Fermi gas of polar molecules, Science **363**, 853 (2019).

[3] M. Duda, X.-Y. Chen, A. Schindewolf, R. Bause, J. von Milczewski, R. Schmidt, I. Bloch, and X.-Y. Luo, Transition from a polaronic condensate to a degenerate Fermi gas of heteronuclear molecules, Nat. Phys. **19**, 720 (2023).

[4] T. Köhler, K. Góral, and P. S. Julienne, Production of cold molecules via magnetically tunable Feshbach resonances, Rev. Mod. Phys. **78**, 1311 (2006).

[5] G. Thalhammer, K. Winkler, F. Lang, S. Schmid, R. Grimm, and J. H. Denschlag, Long-lived Feshbach molecules in a three-dimensional optical lattice, Phys. Rev. Lett. **96**, 050402 (2006).

[6] P. Naidon and S. Endo, Efimov physics: A review, Rep. Prog. Phys. **80**, 056001 (2017).

[7] P. Weckesser, F. Thielemann, D. Wiater, A. Wojciechowska, L. Karpa, K. Jachymski, M. Tomza, T. Walker, and T. Schaetz, Observation of Feshbach resonances between a single ion and ultracold atoms, Nature (London) **600**, 429 (2021).

[8] H. Hirzler, R. S. Lous, E. Trimby, J. Pérez-Ríos, A. Safavi-Naini, and R. Gerritsma, Observation of chemical reactions between a trapped ion and ultracold feshbach dimers, Phys. Rev. Lett. **128**, 103401 (2022).

[9] V. Bendkowsky, B. Butscher, J. Nipper, J. P. Shaffer, R. Löw, and T. Pfau, Observation of ultralong-range Rydberg molecules, Nature (London) **458**, 1005 (2009).

[10] D. Booth, S. Rittenhouse, J. Yang, H. Sadeghpour, and J. Shaffer, Production of trilobite Rydberg molecule dimers

[11] T. Niederprüm, O. Thomas, T. Eichert, C. Lippe, J. Pérez-Ríos, C. H. Greene, and H. Ott, Observation of pendular butterfly Rydberg molecules, Nat. Commun. **7**, 12820 (2016).

[12] C. Fey, F. Hummel, and P. Schmelcher, Ultralong-range Rydberg molecules, Mol. Phys. **118**, e1679401 (2020).

[13] F. Hummel, P. Schmelcher, and M. T. Eiles, Vibronic interactions in trilobite and butterfly Rydberg molecules, Phys. Rev. Res. **5**, 013114 (2023).

[14] F. Hummel, M. T. Eiles, and P. Schmelcher, Synthetic dimension-induced conical intersections in Rydberg molecules, Phys. Rev. Lett. **127**, 023003 (2021).

[15] F. Engel, T. Dieterle, T. Schmid, C. Tomschitz, C. Veit, N. Zuber, R. Löw, T. Pfau, and F. Meinert, Observation of Rydberg blockade induced by a single ion, Phys. Rev. Lett. **121**, 193401 (2018).

[16] T. Schmid, C. Veit, N. Zuber, R. Löw, T. Pfau, M. Tarana, and M. Tomza, Rydberg molecules for ion-atom scattering in the ultracold regime, Phys. Rev. Lett. **120**, 153401 (2018).

[17] F. M. Gambetta, C. Zhang, M. Hennrich, I. Lesanovsky, and W. Li, Long-range multibody interactions and three-body antiblockade in a trapped Rydberg ion chain, Phys. Rev. Lett. **125**, 133602 (2020).

[18] L. Wang, M. Deiß, G. Raithel, and J. H. Denschlag, Optical control of atom-ion collisions using a Rydberg state, J. Phys. B **53**, 134005 (2020).

[19] M. Deiß, S. Haze, and J. Hecker Denschlag, Long-range atom–ion Rydberg molecule: A novel molecular binding mechanism, Atoms **9**, 34 (2021).

[20] A. Duspayev, X. Han, M. A. Viray, L. Ma, J. Zhao, and G. Raithel, Long-range Rydberg-atom–ion molecules of Rb and Cs, Phys. Rev. Res. **3**, 023114 (2021).

[21] N. Zuber, V. S. Anasuri, M. Berngruber, Y.-Q. Zou, F. Meinert, R. Löw, and T. Pfau, Observation of a molecular bond between ions and Rydberg atoms, Nature (London) **605**, 453 (2022).

[22] See Supplemental Material at http://link.aps.org/supplemental/10.1103/PhysRevLett.133.083001 for details of the experimental sequence, dynamics simulations, and additional measurements, which includes Refs. [23–27].

[23] S. Weber, C. Tresp, H. Menke, A. Urvoy, O. Firstenberg, H. P. Büchler, and S. Hofferberth, Calculation of Rydberg interaction potentials, J. Phys. B **50**, 133001 (2017).

[24] T. F. Gallagher, *Rydberg Atoms*, Cambridge Monographs on Atomic, Molecular and Chemical Physics (Cambridge University Press, Cambridge, England, 1994).

[25] D. R. Inglis and E. Teller, Ionic depression of series limits in one-electron spectra, Astrophys. J. **90**, 439 (1939).

[26] H. Köppel, W. Domcke, and L. S. Cederbaum, Multimode molecular dynamics beyond the born-oppenheimer approximation, in *Advances in Chemical Physics* (John Wiley & Sons, Ltd., New York, 1984), Vol. 57, pp. 59–246.

[27] M. Schlagmüller, T. C. Liebisch, F. Engel, K. S. Kleinbach, F. Böttcher, U. Hermann, K. M. Westphal, A. Gaj, R. Löw, S. Hofferberth, T. Pfau, J. Pérez-Ríos, and C. H. Greene, Ultracold chemical reactions of a single Rydberg atom in a dense gas, Phys. Rev. X **6**, 031020 (2016).

[28] C. Zener and R. H. Fowler, Non-adiabatic crossing of energy levels, Proc. R. Soc. A **137**, 696 (1932).

[29] J. R. Rubbmark, M. M. Kash, M. G. Littman, and D. Kleppner, Dynamical effects at avoided level crossings: A study of the Landau-Zener effect using Rydberg atoms, Phys. Rev. A **23**, 3107 (1981).

[30] C. Veit, N. Zuber, O. A. Herrera-Sancho, V. S. V. Anasuri, T. Schmid, F. Meinert, R. Löw, and T. Pfau, Pulsed ion microscope to probe quantum gases, Phys. Rev. X **11**, 011036 (2021).

[31] Y.-Q. Zou, M. Berngruber, V. S. V. Anasuri, N. Zuber, F. Meinert, R. Löw, and T. Pfau, Observation of vibrational dynamics of orientated Rydberg-atom-ion molecules, Phys. Rev. Lett. **130**, 023002 (2023).